Speeding up PET/MR for cancer staging of children and young adults

Maryam Aghighi, MD[1], **Laura Jean Pisani, PhD**[1], **Ziyan Sun, MD**[1], **Christopher Klenk, MD**[1], **Himani Madnawat, MS**[1], **Sandra Luna Fineman, MD**[2], **Ranjana Advani, MD**[3], **Rie Von Eyben, MS**[4], **Daniel Owen, BS**[1], **Andrew Quon, MD**[1], **Michael Moseley, PhD**[1], and **Heike E. Daldrup-Link, MD, PhD**[1]

[1]Department of Radiology, Molecular Imaging Program at Stanford, Stanford University

[2]Department of Pediatrics, Lucile Packard Children's Hospital, Stanford University

[3]Department of Medicine, Stanford Hospital, Stanford University

[4]Department of Radiation and Oncology, Stanford University

Abstract

Objective—Combining ^{18}F-FDG PET with whole-body MR for paediatric cancer staging is practically feasible if imaging protocols can be streamlined. We compared ^{18}F-FDG PET/STIR with accelerated ^{18}F-FDG PET/FSPGR for whole-body tumour imaging in children and young adults.

Methods—Thirty-three children and young adults (17.5±5.5 years, range 10–30 years) with malignant lymphoma or sarcoma underwent a ^{18}F-FDG PET staging exam, followed by ferumoxytol-enhanced STIR and FSPGR whole-body MR. ^{18}F-FDG PET scans were fused with MR data and the number and location of tumours on each integrated exam was determined. Histopathology and follow-up imaging served as standard of reference. The agreement of each MR sequence with the reference and the whole-body imaging times were compared using Cohen's kappa coefficient and student t-test, respectively.

Results—Comparing ^{18}F-FDG PET/FSPGR to ^{18}F-FDG PET/STIR, sensitivities were 99.3% for both, specificities were statistically equivalent, 99.8% versus 99.9% and the agreement with the reference based on Cohen's kappa coefficient was also statistically equivalent, 0.989 versus 0.992. However, the total scan-time for accelerated FSPGR of 19.8±5.3 minutes was significantly shorter compared to 29.0±7.6 minutes for STIR (p=0.001).

Conclusion—[18]F-FDG PET/FSPGR demonstrated equivalent sensitivities and specificities for cancer staging compared to ^{18}F-FDG PET/STIR, but could be acquired with shorter acquisition time.

Keywords

Whole-body PET/MR imaging; PET/CT; Iron Oxide Nanoparticles; STIR; Paediatric Cancer

Corresponding address: Heike E. Daldrup-Link, Molecular Imaging Program at Stanford, Stanford University, 725 Welch Road, Stanford, CA 94304, Telephone number: 650-723-8996, heiked@stanford.edu.

Introduction

Accurate staging of malignant tumours in children and adolescents is critical to estimate prognosis and initiate appropriate cancer treatment [1–3]. ^{18}F-FDG PET/CT exams are the current staging procedure of choice for the majority of paediatric patients with lymphomas and for some patients with sarcomas [4]. However, ^{18}F-FDG PET/CT exams are associated with considerable radiation exposure [5–7]. We recently reported that radiation-free whole-body MRI scans provide equivalent information for cancer staging compared to ^{18}F-FDG PET/CT [8]. While further studies are underway to determine the value of whole-body MRI for treatment monitoring, ^{18}F-FDG PET/MR studies can provide an interim alternative for tumour re-staging through an imaging process that exposes young patients to significantly less radiation than PET/CT and includes metabolic and anatomic information for therapy response assessment [9, 10]. A recent study reported that co-registration of ^{18}F-FDG PET data with MR scans instead of CT scans allowed for whole-body staging of children with 80% reduced radiation exposure. However, previous PET/MR whole-body staging protocols for children were limited by using T2-weighted sequences for anatomical co-registration of PET data, which led to significantly increased scan times compared to a PET/CT exam [11]. Although PET/MRI offers improved soft tissue contrast compared to CT [12–15] and allows for primary tumour and whole-body staging in one session [16], two potential concerns have previously inhibited implementation of faster T1-weighted sequences: (1) Inability to delineate vessels over the duration of a whole-body scan due to contrast extravasation and (2) misaligned PET data co-registration on breath-hold scans after deep inspiration.

We propose to solve these problems by using the blood pool agent ferumoxytol for long-lasting vascular enhancement and end-expiration breath-hold T1-weighted sequences for co-registration with ^{18}F-FDG PET data. Ferumoxytol is an FDA-approved iron supplement composed of ultra-small super-paramagnetic iron oxide nanoparticles which can be used "off label" as a contrast agent for MR imaging [17–20]. The goal of our study was to compare the time-efficiency, cost-efficiency and diagnostic accuracy of fused ^{18}F-FDG PET/STIR and ^{18}F-FDG PET/FSPGR exams for whole-body tumour staging. Through our analysis, we have concluded that ferumoxytol-enhanced breath-hold T1-weighted fast spoiled gradient recalled echo (FSPGR) scans substantially expedite acquisition of anatomical background information, improve diagnostic cost-efficiency, and provide equal imaging specificity and sensitivity for whole-body PET/MR staging of paediatric patients and young adults. This reduction in image acquisition time makes the ^{18}F-FDG PET/FSPGR exam a clinically feasible, radiation-free staging alternative for diagnosing children and young adults with cancer.

Materials and Methods

Patients

This prospective, non-randomized study was approved by the institutional review board (IRB = local ethical committee) and the Cancer Center at our institution and written informed consent was obtained from all individual participants and their parents (in case of minors) included in the study. We investigated 33 patients with malignant lymphomas (n = 27) and malignant sarcomas (n = 6) including 24 males and 9 females with a mean age of

17.5 ± 5.5 years (range 10 to 30 years) as shown in Table 1 with age, gender and tumour type of all patients. Twenty one of the 33 patients were part of a previously reported study on whole-body diffusion-weighted MRI. To provide accelerated cancer staging, the goal of our current study was to compare the sensitivities and specificities of two different PET/MR techniques for cancer staging, namely [18]FFDG PET/FSPGR and ^{18}F-FDG PET/STIR sequences. Inclusion criteria comprised (1) age between 8 and 30 years (2) newly diagnosed lymphoma or sarcoma and (3) scheduled or completed ^{18}F-FDG PET/CT. All tumours were evaluated before start of therapy. The lower age threshold of eight years was chosen to avoid the need of sedation or anaesthesia. Exclusion criteria comprised (1) MR-incompatible metal implants, (2) claustrophobia (3) hemosiderosis/hemochromatosis and (4) history of allergies against iron products or any history of severe anaphylactic reactions.

^{18}F-FDG PET/CT

All patients underwent clinical standard ^{18}F-FDG PET/CT scans for tumour staging on a Discovery LS 690 PET/CT scanner (GE Healthcare). The patients fasted at least six hours before the ^{18}F-FDG scan and blood glucose levels were confirmed to be less than 150 mg/dl at the time of the ^{18}F-FDG injection. Approximately 60 min after injection of 0.33 GBq ± 0.12 GBq ^{18}F-FDG, an emission PET was acquired of the whole-body. PET images were attenuation corrected by low dose CT data, reconstructed with a standard iterative algorithm and reformatted into axial, coronal, and sagittal views.

Whole-body MR Imaging

MR imaging was performed on a 3T Discovery 750 magnetic resonance scanner (GE Healthcare). We obtained investigational new drug approval from the FDA (IND111,154) to use the FDA-approved iron supplement ferumoxytol (Feraheme™, Fe5874 O8752-C11719 H18682 O9933 Na414; AMAG Pharmaceuticals, Inc.) [21] "off-label" as a contrast agent for MR imaging in children and young adults. Ferumoxytol is composed of semi-synthetic carbohydrate-coated super paramagnetic iron oxide nanoparticles with a molecular weight of 731 kDa, a hydrodynamic particle diameter of 30 nm [22], and a long plasma half-life of 15 hours. Due to their super-paramagnetic properties, ferumoxytol nanoparticles give positive contrast on T1-weighted MR images and negative contrast on T2-weighted MR images [23]. All patients received an intravenous injection of ferumoxytol at a dose of 5 mg Fe/kg body weight before their MRI scan over a minimum of 15 minutes. [24] A personalized approach was used to ensure minimal scan time for every patient. Before the scan, each patient practiced guided breath-holding and we recorded their maximum breath-hold interval, which ranged between 20–35 seconds. The minimal field-of-view (FOV) that encompassed the patient was used, which ranged from 20–50 cm. Repetition times (TR) and echo times (TE) were adjusted to ensure a constant signal-to-noise ratio for all patients. Breath-hold fat-saturated T1-weighted fast spoiled gradient recalled echo (FSPGR) sequences were obtained with a flip angle of 15°, a TR of 7–12 ms, a TE of 1–3 ms and an acceleration factor of 2. This parallel imaging acceleration required Array Spatial Sensitivity Encoding Technique (ASSET) calibration. Short TI inversion recovery (STIR) sequences were obtained with a TR of 4000–8000 ms and a TE of 50–60 ms. All sequences were obtained with a single acquisition, a bandwidth of 31 kHz, a slice thickness of 4–5 mm, and an image matrix of 256×192. Voxel dimensions amongst our acquisitions did not exceed 2.5 mm in-plane by 5

mm through-plane, and were sufficiently small to detect lymph nodes that met the clinical criterion for radiological diagnosis (15 mm mediastinal and 10 mm superficial lymph nodes).

To generate whole-body images that integrate the functional and anatomic information of the acquired ^{18}F-FDG and whole-body MRI scans, we post-processed our images using OsiriX software [25]. ^{18}F-FDG PET images were colour-rendered by applying the 'PET' CLUT followed by fusion with gray-scale ferumoxytol-enhanced anatomical STIR and T1-weighted FSPGR images.

Data Analysis

In order to compare fused ^{18}F-FDG PET/STIR and ^{18}F-FDG PET/FSPGR exams, all images were interpreted by consensus between an experienced radiologist and an experienced nuclear medicine physician. ^{18}F-FDG PET/STIR and ^{18}F-FDG PET/FSPGR scans of each patient were evaluated in random order in separate sessions, which were separated by at least two months in order to avoid recall bias. In order to further minimize recall bias, the reviewers were blinded to histopathology, staging outcome, disease history and other imaging findings. Histopathology, as well as clinical and imaging follow up for at least 6 months served as the standard of reference. All primary tumours were confirmed by histopathology. Sixty two regions assessed in each patient (n = 33) are specified as:

- Nodal regions (N1–33):

  – Head/neck (H1–5): Waldeyer's ring, bilateral cervical, and bilateral supraclavicular

  – Chest (C1–11): bilateral infraclavicular, prevascular, aortopulmonary, paratracheal, pretracheal, subcarinal, posterior mediastinal, bilateral hilar, and retrocrural

  – Axilla/extremities (Ax1–2): bilateral axillary

  – Abdomen (Ab1–7): gastrohepatic, periportal, aortocaval, retrocrural, mesenteric, retroperitoneal, and paraaortic

  – Pelvis (P1–8): bilateral common iliac, bilateral internal iliac, bilateral external iliac, and bilateral inguinal

- Extra-nodal regions (E1–10): bilateral pleura, bilateral lung, bilateral breast, myocardium, spleen, liver, and bowel

- Bone regions (B1–19): cervical spine, bilateral clavicle, bilateral scapula, bilateral rib, thoracic spine, bilateral humerus, sternum, bilateral pelvis, bilateral femur, tibia, sacrum, lumbar spine, and coccyx

Based on regional analysis, sensitivities, specificities, positive predictive values, negative predictive values and diagnostic accuracies were calculated for ^{18}F-FDG PET/STIR and efficient ^{18}F-FDG PET/FSPGR exams. The Cohen's kappa statistic was evaluated to determine the level of agreement between the ^{18}F-FDG PET/STIR and ^{18}F-FDG PET/FSPGR methods and the standard of reference. Cohen kappa coefficients of 1 or 0 indicate

complete agreement or no more agreement than can be expected to occur by chance alone, respectively.

In addition, whole-body image acquisition times were recorded for each patient as: a) the MR scan-time per single anatomical site, the total whole-body scan-time as well as b) the combined time for coil placement, localizer sequence, ASSET calibration and whole-body MR sequence. Mean acquisition times for ^{18}F-FDG PET/STIR and ^{18}F-FDG PET/FSPGR scans were compared with a student's t-test with a significance threshold of 0.05.

Results

The reviewers successfully detected 285 malignant lesions in 2046 anatomical regions (62 regions in 33 patients). Ferumoxytol-enhanced ^{18}F-FDG PET/FSPGR exams provided a similar visual representation of pediatric tumors compared with ^{18}F-FDG PET/STIR exams as shown for a 25-year-old patient with Hodgkin's lymphoma with mediastinal lymph node (Fig. 1).

^{18}F-FDG PET/FSPGR detected 286 lesions, including 205 nodal lesions, 58 bone lesions and 23 extra-nodal lesions. ^{18}F-FDG PET/STIR identified 285 lesions, including 205 nodal lesions, 57 bone lesions and 23 extra-nodal lesions. ^{18}F-FDG PET/FSPGR revealed 3 false positive findings, 2 false negative, 283 true positive and 1380 true negative lesions. ^{18}F-FDG PET/STIR diagnosed 2 false positive and 2 false negative lesions, 283 true positive and 1381 true negative lesions. False negative findings included one bone lesion and one lung nodule as shown in Fig. 2. False positive lesions included physiological bowel uptake on PET (n = 1), inflammatory lymph nodes (n = 1) and hypercellular hematopoietic marrow (n = 1). False positive lesions on ^{18}F-FDG PET/FSPGR, but not ^{18}F-FDG PET/STIR included hypermetabolic hematopoietic bone marrow on ^{18}F-FDG PET, which showed normal homogenous ferumoxytol-enhancement on STIR images and was confirmed as normal bone marrow by bone marrow biopsy (Fig. 3).

Sensitivity and specificity were 99.3% and 99.8% for ^{18}F-FDG PET/FSPGR and 99.3% and 99.9% for ^{18}F-FDG PET/STIR imaging, respectively. The positive predictive value was 99.0% for ^{18}F-FDG PET/FSPGR and 99.3% for ^{18}F-FDG PET/STIR (Table 2). Based on Cohen's kappa coefficient, the agreement with the standard of reference was 0.989 for ^{18}F-FDG PET/FSPGR and 0.992 for ^{18}F-FDG PET/STIR.

The imaging time for the whole-body scan was significantly shorter using accelerated FSPGR sequences (19.8 ± 5.3 minutes with pure MR scan-time of 2.5 ± 0.7 minutes) as opposed to STIR images (29.0 ± 7.6 minutes with pure MR scan-time of 16.2 ± 4.7 minutes; p = 0.001). Fig. 4(a) shows the total scan-time for FSPGR and STIR scans. Fig. 4(b) demonstrates that the scan-time per anatomical site for accelerated FSPGR (0.52 ± 0.07 minutes) is considerably shorter than STIR (6.2 ± 0.9 minutes), p < 0.001. In addition, the time for localizer, coil placement, ASSET calibration and pure MR scan are illustrated in Fig. 4(c).

The imaging cost in our institution for whole-body MR scan is $627 per hour plus $70 per exam, thus accelerated FSPGR sequences costs on average 19.8 min × $627/hour + $70 =

$276.91 which is less than STIR that costs on average 29.0 min $\times$ $627/hour + $70 = $373.05.

Discussion

Different sequences are typically used in whole-body MR imaging for monitoring tumours in children and young adults, including STIR, T2-weighted fast spin-echo sequences, diffusion-weighted images (DWI), and gadolinium-enhanced T1-weighted gradient echo sequences. STIR has been the most commonly used sequence in whole-body MR imaging and can be performed in less than 30 minutes [26–28]. Our data show that ferumoxytol-enhanced ^{18}F-FDG PET/FSPGR exams provide equal sensitivity and specificity compared to ^{18}F-FDG PET/STIR exams with improved time- and cost-efficiency. PET/MR combines the high anatomical resolution and soft tissue contrast of MRI with the high sensitivity of PET, thereby overcoming the limited sensitivity of traditional MRI approaches and concerns regarding radiation exposure of paediatric patients from PET/CT scans [29–32]. Through these benefits, patient quality of life (QoL) is purportedly enhanced by providing equivalent diagnostic information with reduced patient dose.

We acquired MR images after administration of the iron supplement ferumoxytol, in order to achieve long lasting blood pool enhancement of vessels throughout the duration of the whole body scan. [8]. Perhaps one could compare this to adding a diagnostic CT to a PET/CT, which was traditionally done with low dose scans for attenuation correction only. Ferumoxytol is a "blood pool agent" and has a blood half-life of 15 hours in humans, which allows for long lasting vessel enhancement on MR images [33]. Therefore, it is not crucial for the quality of the imaging scan to administer the contrast agent while the patient is in the scanner or to start a post-contrast scan immediately after contrast media administration. This is a convenient feature for clinical applications in paediatric patients, where timing of contrast agent injections and scanning cannot always be reliably planned.

Integrated PET/MR scanners are expensive and may not be affordable for many paediatric imaging centres. Our data also show that image registration of sequentially acquired ^{18}F-FDG PET and MR scans is a feasible alternative. The proposed breath-hold T1-weighted SPGR sequence can be equally used to expedite whole-body MRI data acquisition of sequential or integrated PET/MR technologies. We utilized OsiriX for image data fusion which allows for image co-registration within less than 500 microns [34]. Others have confirmed the feasibility of this approach [35–37]. Using sequential imaging approaches takes advantage of CT-based attenuation correction of PET data, while integrated scans require MR-based attenuation correction. Our ongoing studies on an integrated PET/MR scanner confirm that the same approach described here can be used for fused ferumoxytol-enhanced ^{18}F-FDG PET/MR scans.

Both ferumoxytol-enhanced T1-weighted FSPGR and STIR sequences have some limitations due to specific artefacts: On STIR images, ghosting artefacts from breath motion in the single-average acquisition was noted. On the T1-weighted FSPGR images during breath hold, cardiac motion artefacts were apparent, but more confined than the pervasive ghosting from the free breathing acquisition. Using large field-of-views for whole body

scanning may lead to incomplete fat saturation at the edge of the coil. Also, the calibration and ASSET scans can in principle cause uncorrected aliasing and reduce SNR, although we did not encounter any major artefacts of this nature.

Of note, we injected ferumoxytol directly before the MRI scans. This was technically convenient and provided strong vascular enhancement, similar to the procedure of a contrast-enhanced CT scan. Our previous studies showed that the vascular enhancement improved tumour delineation compared to unenhanced scans [8]. However, this relatively early post-contrast time point was too early to achieve enhancement of tumours or lymph nodes, which is strongest at 24 hours post injection [38, 39]. Further studies are needed to determine whether the added diagnostic information for lymph node characterization justifies a two-step visit (day one for contrast injection and day 2 for MRI).

Our proposed approach requires injection of an iron oxide nanoparticle compound. The European radiological community has extensive clinical experience with these compounds and our team has applied various iron oxide nanoparticle compounds as MR contrast agents in phase I–IV clinical trials [40–44]. These agents are generally well tolerated and show excellent safety profiles [45–48]. Considering a ferumoxytol dose of 5 mg/kg and a concentration of 30 mg Fe/ml, we anticipate injecting 250–400 mg Fe in a young adult with an average body weight of 50–80 kg (of note, these are coated iron particles, not free iron). This iron dose is lower than the FDA-approved ferumoxytol dose for anaemia treatment and comparable to the iron dose administered with one blood transfusion. Anaphylaxis or anaphylactoid reactions to ferumoxytol were reported in 0.1–0.2% of exposed adult patients, which is comparable to other MR contrast agents. Ferumoxytol is not excreted via the kidneys and thus, not associated with any risk of nephrogenic sclerosis (a potential adverse event with Gd-chelates) [19, 49, 50]. In addition, ferumoxytol may represent al alternative to the recently reported deposition of Gd-chelates in the brain [51], although no comparative information is available so far regarding ferumoxytol deposition in the brain. Iron oxide nanoparticles are not approved for clinical use in children and applications in the US are done through an investigational new drug (IND) application with the FDA. Safety data in paediatric patients are limited, but have not shown clinically significant side effects so far [52, 53]. The recently renewed safety discussion around iron products does not relate to new toxic effects [24], but has to be taken seriously and has led to a black box warning by the FDA. Our team currently investigates the underlying pathophysiology of anaphylactic reactions to iron oxide nanoparticles, which will hopefully enable preventive actions in the future.

Although recent advances in MRI sequences for pulmonary imaging do allow for detection of pulmonary nodules, there is a potential to miss small pulmonary lesions on MR scans which are more conspicuous with CT. Previous investigators' findings are in accordance with our results [54, 55]. Future technical improvements may overcome this limitation [56, 57].

Focal and multifocal bone marrow infiltration shows only a minor or no iron oxide uptake, while normal hematopoietic bone marrow shows substantial iron oxide uptake. Therefore, normal and neoplastic marrow can be differentiated on ferumoxytol-enhanced STIR images,

which can help to correctly identify false positive, hypermetabolic hematopoietic bone marrow on PET scans. The bone marrow iron enhancement is detectable over a wide range of magnetic field strengths, from 1.5 to 7 Tesla [58].

We recently reported a radiation-free approach for whole-body tumour staging with MRI which relied on fusion of colour-encoded diffusion-weighted (DW) MRI sequences with anatomical FSPGR sequences [8]. To date, clinical decisions rely on metabolic information from ^{18}F-FDG PET scans for monitoring of paediatric lymphomas [59–64]. Thus, while the medical community is in the process of assessing the value of diffusion-weighted sequences and apparent diffusion coefficients (ADC values) for treatment monitoring of paediatric lymphomas, ^{18}F-FDG PET/MR with accelerated acquisition protocols may represent a compromise toward accurate diagnoses with the least possible radiation exposure.

Conclusion

We increased the time- and cost-efficiency of whole-body PET/MR scans by replacing traditional STIR scans with contrast-enhanced, breath-hold T1-weighted FSPGR scans. This efficient imaging approach improved the feasibility of PET/MR as a monitoring option for paediatric tumours, with reduced radiation exposure compared to PET/CT.

Acknowledgments

References

1. Federman N, Feig SA. PET/CT in evaluating pediatric malignancies: a clinician's perspective. Journal of Nuclear Medicine. 2007; 48:1920–1922. [PubMed: 18056331]

2. Gerth HU, Juergens KU, Dirksen U, Gerss J, Schober O, Franzius C. Significant benefit of multimodal imaging: PET/CT compared with PET alone in staging and follow-up of patients with Ewing tumors. Journal of Nuclear Medicine. 2007; 48:1932–1939. [PubMed: 18006618]

3. Kleis M, Daldrup-Link H, Matthay K, Goldsby R, Lu Y, Schuster T, et al. Diagnostic value of PET/CT for the staging and restaging of pediatric tumors. European journal of nuclear medicine and molecular imaging. 2009; 36:23–36. [PubMed: 18719909]

4. Tatsumi M, Miller JH, Wahl RL. 18F-FDG PET/CT in evaluating non-CNS pediatric malignancies. J Nucl Med. Dec.2007 48:1923–31. [PubMed: 18056332]

5. Brenner DJ, Hall EJ. Computed tomography--an increasing source of radiation exposure. N Engl J Med. Nov 29.2007 357:2277–84. [PubMed: 18046031]

6. Hall E, Brenner D. Cancer risks from diagnostic radiology. Cancer. 2008; 81

7. Robbins E. Radiation risks from imaging studies in children with cancer. Pediatric blood & cancer. 2008; 51:453–457. [PubMed: 18465805]

8. Klenk C, Gawande R, Uslu L, Khurana A, Qiu D, Quon A, et al. Ionising radiation-free whole-body MRI versus (18)F-fluorodeoxyglucose PET/CT scans for children and young adults with cancer: a

prospective, non-randomised, single-centre study. Lancet Oncol. Mar.2014 15:275–85. [PubMed: 24559803]

9. Doot RK, McDonald ES, Mankoff DA. Role of PET quantitation in the monitoring of cancer response to treatment: review of approaches and human clinical trials. Clinical and Translational Imaging. 2014; 2:295–303. [PubMed: 25229053]

10. Schwarzenberg J, Czernin J, Cloughesy TF, Ellingson BM, Pope WB, Grogan T, et al. Treatment response evaluation using 18F-FDOPA PET in patients with recurrent malignant glioma on bevacizumab therapy. Clinical Cancer Research. 2014

11. Hirsch FW, Sattler B, Sorge I, Kurch L, Viehweger A, Ritter L, et al. PET/MR in children. Initial clinical experience in paediatric oncology using an integrated PET/MR scanner. Pediatric radiology. 2013; 43:860–875. [PubMed: 23306377]

12. Vargas MI, Becker M, Garibotto V, Heinzer S, Loubeyre P, Gariani J, et al. Approaches for the optimization of MR protocols in clinical hybrid PET/MRI studies. Magnetic Resonance Materials in Physics, Biology and Medicine. 2013; 26:57–69.

13. Yankeelov TE, Peterson TE, Abramson RG, Garcia-Izquierdo D, Arlinghaus LR, Li X, et al. Simultaneous PET–MRI in oncology: a solution looking for a problem? Magnetic resonance imaging. 2012; 30:1342–1356. [PubMed: 22795930]

14. Loevner LA, Kim AK, Mikityansky I. PET/CT-MR Imaging in Head and Neck Cancer Including Pitfalls and Physiologic Variations. PET Clinics. 2008; 3:335–353. [PubMed: 27156665]

15. Seiboth L, Van Nostrand D, Wartofsky L, Ousman Y, Jonklaas J, Butler C, et al. Utility of PET/ neck MRI digital fusion images in the management of recurrent or persistent thyroid cancer. Thyroid. 2008; 18:103–111. [PubMed: 18279011]

16. Littooij AS, Torigian DA, Kwee TC, de Keizer B, Alavi A, Nievelstein RA. Potential Clinical Applications of PET/Magnetic Resonance Imaging. PET Clinics. 2013; 8:367–384. [PubMed: 27158074]

17. Landry R, Jacobs PM, Davis R, Shenouda M, Bolton WK. Pharmacokinetic study of ferumoxytol: a new iron replacement therapy in normal subjects and hemodialysis patients. Am J Nephrol. Jul-Aug;2005 25:400–10. [PubMed: 16088081]

18. Li W, Tutton S, Vu AT, Pierchala L, Li BS, Lewis JM, et al. First-pass contrast-enhanced magnetic resonance angiography in humans using ferumoxytol, a novel ultrasmall superparamagnetic iron oxide (USPIO)-based blood pool agent. J Magn Reson Imaging. Jan.2005 21:46–52. [PubMed: 15611942]

19. Lu M, Cohen MH, Rieves D, Pazdur R. FDA report: Ferumoxytol for intravenous iron therapy in adult patients with chronic kidney disease. Am J Hematol. May.2010 85:315–9. [PubMed: 20201089]

20. Aghighi M, Golovko D, Ansari C, Marina NM, Pisani L, Kurlander L, et al. Imaging Tumor Necrosis with Ferumoxytol. PLoS ONE. 2015; 10:e0142665. [PubMed: 26569397]

21. AMAG Pharmaceuticals, Inc. Feraheme (ferumoxytol) package insert. Lexington, MA: 2009.

22. Balakrishnan VS, Rao M, Kausz AT, Brenner L, Pereira BJ, Frigo TB, et al. Physicochemical properties of ferumoxytol, a new intravenous iron preparation. Eur J Clin Invest. Jun.2009 39:489–96. [PubMed: 19397688]

23. Neuwelt EA, Hamilton BE, Varallyay CG, Rooney WR, Edelman RD, Jacobs PM, et al. Ultrasmall superparamagnetic iron oxides (USPIOs): a future alternative magnetic resonance (MR) contrast agent for patients at risk for nephrogenic systemic fibrosis (NSF)? Kidney Int. Mar.2009 75:465–74. [PubMed: 18843256]

24. FDA. Safety Announcement, Drug Safety Communication. FDA strengthens warnings and changes prescribing instructions to decrease the risk of serious allergic reactions with anemia drug Feraheme (ferumoxytol). 2015.

25. Rosset A, Spadola L, Ratib O. OsiriX: an open-source software for navigating in multidimensional DICOM images. J Digit Imaging. Sep.2004 17:205–16. [PubMed: 15534753]

26. Teixeira SR, Elias J Junior, Nogueira-Barbosa MH, Guimarães MD, Marchiori E, Santos MK. Whole-body magnetic resonance imaging in children: state of the art. Radiologia brasileira. 2015; 48:111–120. [PubMed: 25987752]

27. Chavhan GB, Babyn PS. Whole-body MR imaging in children: principles, technique, current applications, and future directions. Radiographics. 2011; 31:1757–1772. [PubMed: 21997993]

28. Kellenberger CJ, Miller SF, Khan M, Gilday DL, Weitzman S, Babyn PS. Initial experience with FSE STIR whole-body MR imaging for staging lymphoma in children. European radiology. 2004; 14:1829–1841. [PubMed: 15365752]

29. Balyasnikova S, Lofgren J, de Nijs R, Zamogilnaya Y, Hojgaard L, Fischer BM. PET/MR in oncology: an introduction with focus on MR and future perspectives for hybrid imaging. Am J Nucl Med Mol Imaging. 2012; 2:458–74. [PubMed: 23145362]

30. Drzezga A, Souvatzoglou M, Eiber M, Beer AJ, Furst S, Martinez-Moller A, et al. First clinical experience with integrated whole-body PET/MR: comparison to PET/CT in patients with oncologic diagnoses. J Nucl Med. Jun.2012 53:845–55. [PubMed: 22534830]

31. Herzog H, Van Den Hoff J. Combined PET/MR systems: an overview and comparison of currently available options. Q J Nucl Med Mol Imaging. Jun.2012 56:247–67. [PubMed: 22695336]

32. Platzek I, Beuthien-Baumann B, Langner J, Popp M, Schramm G, Ordemann R, et al. PET/MR for therapy response evaluation in malignant lymphoma: initial experience. MAGMA. Feb.2013 26:49–55. [PubMed: 22983794]

33. Simon GH, von Vopelius-Feldt J, Fu Y, Schlegel J, Pinotek G, Wendland MF, et al. Ultrasmall supraparamagnetic iron oxide-enhanced magnetic resonance imaging of antigen-induced arthritis: a comparative study between SHU 555 C, ferumoxtran-10, and ferumoxytol. Invest Radiol. Jan. 2006 41:45–51. [PubMed: 16355039]

34. Mandel M, Amorim R, Paiva W, Prudente M, Teixeira MJ, Andrade AFd. 3D Preoperative Planning in the ER with OsiriX®: When There is No Time for Neuronavigation. Sensors. 2013; 13:6477–6491. [PubMed: 23681091]

35. Andersen FL, Ladefoged CN, Beyer T, Keller SH, Hansen AE, Højgaard L, et al. Combined PET/MR imaging in neurology: MR-based attenuation correction implies a strong spatial bias when ignoring bone. Neuroimage. 2014; 84:206–216. [PubMed: 23994317]

36. Antonica F, Asabella AN, Ferrari C, Rubini D, Notaristefano A, Nicoletti A, et al. Useful diagnostic biometabolic data obtained by PET/CT and MR fusion imaging using open source software. Hellenic journal of nuclear medicine. 2014:50. [PubMed: 24392469]

37. Matthew DJ, Linda CT, Leena K, Yasser MMM, Nandita G-T. Co-registration of sequential multidetector computed tomography studies for the evaluation of surgical instrumentation following resection of spinal tumors. Case reports in radiology. 2011; 2011

38. Daldrup-Link HE, Golovko D, Ruffell B, DeNardo DG, Castaneda R, Ansari C, et al. MRI of tumor-associated macrophages with clinically applicable iron oxide nanoparticles. Clinical Cancer Research. 2011; 17:5695–5704. [PubMed: 21791632]

39. Barentsz JO, Fütterer JJ, Takahashi S. Use of ultrasmall superparamagnetic iron oxide in lymph node MR imaging in prostate cancer patients. European journal of radiology. 2007; 63:369–372. [PubMed: 17689215]

40. Daldrup-Link HE, Kaiser A, Link TM, Settles M, Helbich T, Werner M, et al. Comparison between gadopentetate and feruglose (Clariscan)-enhanced MR-mammography: preliminary clinical experience. Acad Radiol. Aug; 2002 9(Suppl 2):S343–7. [PubMed: 12188270]

41. Daldrup-Link HE, Rummeny EJ, Ihssen B, Kienast J, Link TM. Iron-oxide-enhanced MR imaging of bone marrow in patients with non-Hodgkin's lymphoma: differentiation between tumor infiltration and hypercellular bone marrow. Eur Radiol. Jun.2002 12:1557–66. [PubMed: 12042968]

42. Daldrup-Link HE, Brasch RC. Macromolecular contrast agents for MR mammography: current status. Eur Radiol. Feb.2003 13:354–65. [PubMed: 12599002]

43. Daldrup-Link HE, Kaiser A, Helbich T, Werner M, Bjornerud A, Link TM, et al. Macromolecular contrast medium (feruglose) versus small molecular contrast medium (gadopentetate) enhanced magnetic resonance imaging: differentiation of benign and malignant breast lesions. Acad Radiol. Nov.2003 10:1237–46. [PubMed: 14626298]

44. Daldrup-Link HE, Mohanty A, Cuenod C, Pichler B, Link T. New perspectives on bone marrow contrast agents and molecular imaging. Semin Musculoskelet Radiol. Jun.2009 13:145–56. [PubMed: 19455477]

45. Daldrup-Link HE, Rydland J, Helbich TH, Bjornerud A, Turetschek K, Kvistad KA, et al. Quantification of breast tumor microvascular permeability with feruglose-enhanced MR imaging: initial phase II multicenter trial. Radiology. Dec.2003 229:885–92. [PubMed: 14576446]

46. Simon G, Link TM, Wortler K, Doebereiner F, Schulte-Frohlinde E, Daldrup-Link H, et al. Detection of hepatocellular carcinoma: comparison of Gd-DTPA- and ferumoxides-enhanced MR imaging. Eur Radiol. May.2005 15:895–903. [PubMed: 15800773]

47. Metz S, Lohr S, Settles M, Beer A, Woertler K, Rummeny EJ, et al. Ferumoxtran-10-enhanced MR imaging of the bone marrow before and after conditioning therapy in patients with non-Hodgkin lymphomas. Eur Radiol. Mar.2006 16:598–607. [PubMed: 16284770]

48. Spinowitz BS, Kausz AT, Baptista J, Noble SD, Sothinathan R, Bernardo MV, et al. Ferumoxytol for treating iron deficiency anemia in CKD. J Am Soc Nephrol. Aug.2008 19:1599–605. [PubMed: 18525001]

49. Coyne DW. Ferumoxytol for treatment of iron deficiency anemia in patients with chronic kidney disease. Expert Opin Pharmacother. Oct.2009 10:2563–8. [PubMed: 19708851]

50. Schwenk MH. Ferumoxytol: a new intravenous iron preparation for the treatment of iron deficiency anemia in patients with chronic kidney disease. Pharmacotherapy. Jan.2010 30:70–9. [PubMed: 20030475]

51. Schlaudecker JD, Bernheisel CR. Gadolinium-associated nephrogenic systemic fibrosis. American family physician. 2009; 80:711–4. [PubMed: 19817341]

52. Hassan N, Cahill J, Rajasekaran S, Kovey K. Ferumoxytol infusion in pediatric patients with gastrointestinal disorders: first case series. Ann Pharmacother. Dec.2011 45:e63. [PubMed: 22116997]

53. Muehe AM, Feng D, von Eyben R, Luna-Fineman S, Link MP, Muthig T, et al. Safety Report of Ferumoxytol for Magnetic Resonance Imaging in Children and Young Adults. Investigative radiology. 2015

54. Hochhegger B, Marchiori E, Irion K, Moreira J, Zanetti G. MRI in assessment of lung cancer. Thorax. Apr.2011 66:357. [PubMed: 21310757]

55. Chandarana H, Heacock L, Rakheja R, DeMello LR, Bonavita J, Block TK, et al. Pulmonary nodules in patients with primary malignancy: comparison of hybrid PET/MR and PET/CT imaging. Radiology. Sep.2013 268:874–81. [PubMed: 23737537]

56. Sommer G, Koenigkam-Santos M, Biederer J, Puderbach M. Role of MRI for detection and characterization of pulmonary nodules. Der Radiologe. 2014

57. Kurihara Y, Matsuoka S, Yamashiro T, Fujikawa A, Matsushita S, Yagihashi K, et al. MRI of Pulmonary Nodules. American Journal of Roentgenology. 2014; 202:W210–W216. [PubMed: 24555616]

58. Daldrup-Link HE, Rummeny EJ, Ihssen B, Kienast J, Link TM. Iron-oxide-enhanced MR imaging of bone marrow in patients with non-Hodgkin's lymphoma: differentiation between tumor infiltration and hypercellular bone marrow. European radiology. 2002; 12:1557–1566. [PubMed: 12042968]

59. Lin C, Itti E, Haioun C, Petegnief Y, Luciani A, Dupuis J, et al. Early 18F-FDG PET for prediction of prognosis in patients with diffuse large B-cell lymphoma: SUV-based assessment versus visual analysis. Journal of Nuclear Medicine. 2007; 48:1626–1632. [PubMed: 17873129]

60. Haioun C, Itti E, Rahmouni A, Brice P, Rain J-D, Belhadj K, et al. [18F] fluoro-2-deoxy-D-glucose positron emission tomography (FDG-PET) in aggressive lymphoma: an early prognostic tool for predicting patient outcome. Blood. 2005; 106:1376–1381. [PubMed: 15860666]

61. Avril NE, Weber WA. Monitoring response to treatment in patients utilizing PET. Radiologic clinics of North America. 2005; 43:189–204. [PubMed: 15693656]

62. Hoekstra C, Paglianiti I, Hoekstra O, Smit E, Postmus P, Teule G, et al. Monitoring response to therapy in cancer using [18F]-2-fluoro-2-deoxy-D-glucose and positron emission tomography: an overview of different analytical methods. European journal of nuclear medicine. 2000; 27:731–743. [PubMed: 10901462]

63. Kumar R, Maillard I, Schuster SJ, Alavi A. Utility of fluorodeoxyglucose-PET imaging in the management of patients with Hodgkin's and non-Hodgkin's lymphomas. Radiologic Clinics of North America. 2004; 42:1083–1100. [PubMed: 15488559]

64. Allen-Auerbach M, de Vos S, Czernin J. The Impact of Fluorodeoxyglucose–Positron Emission Tomography in Primary Staging and Patient Management in Lymphoma Patients. Radiologic Clinics of North America. 2008; 46:199–211. [PubMed: 18619376]
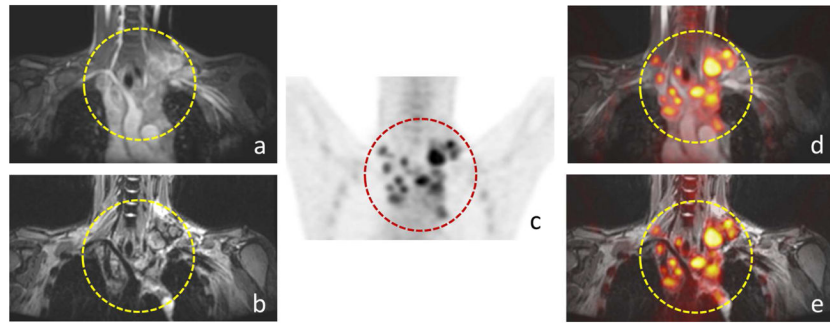
Key Points

Breath-hold FSPGR sequences shorten the data acquisition time for whole-body MR and PET/MR.

Ferumoxytol provides long lasting vascular contrast for whole-body MR and PET/MR.

^{18}F-FDG PET/FSPGR data provided equal sensitivity and specificity for cancer staging compared to ^{18}F-FDG PET/STIR.

Fig. 1.
Comparison of ferumoxytol-enhanced ^{18}F-FDG PET/STIR and ^{18}F-FDG PET/FSPGR exams for the detection of lymph nodes in a 25-year-old patient with Hodgkin's lymphoma: Positive mediastinal lymph nodes are noted (circle) on coronal (a) FSPGR, (b) STIR, (c) ^{18}F-FDG PET as well as (d) fused ^{18}F-FDG PET/FSPGR, (e) PET/STIR exams.
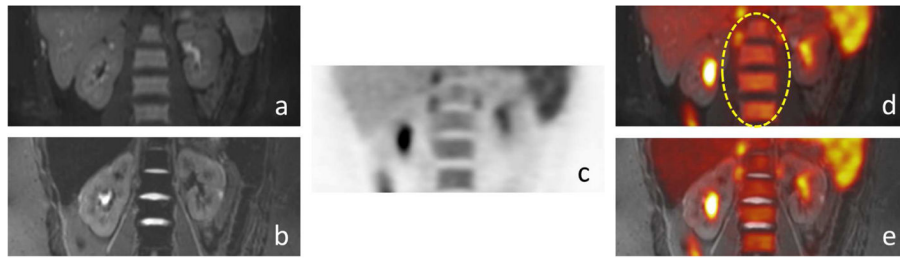
Fig. 2.
False negative lung nodule in a 16-year-old patient with lymphoma on axial (a) CT shows a lung nodule close to the diaphragm (circle), (b) ^{18}F-FDG PET/CT shows no significant FDG update, (c) FSPGR, (d) ^{18}F-FDG PET/FSPGR, (e) STIR, (f) ^{18}F-FDG PET/STIR exam show equivalent information, (g) ^{18}F-FDG PET.
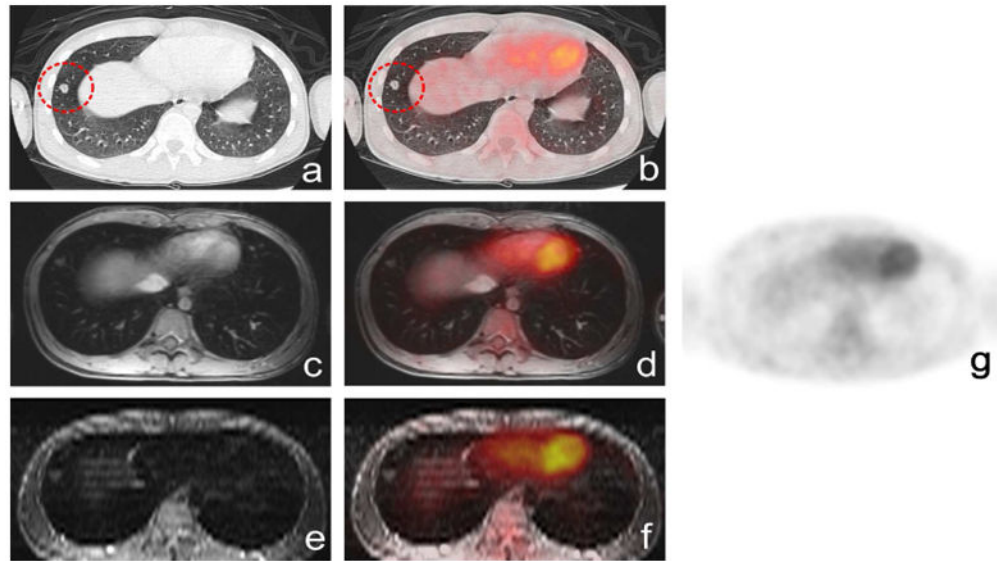
Fig. 3.
False positive, biopsy proven normal hypercellular hematopoietic marrow in a 15-year-old patient with lymphoma: (a) coronal ferumoxytol-enhanced FSPGR(b) coronal STIR scans show homogenous negative (dark) ferumoxytol-enhancement, confirming normal marrow, (c) hypermetabolic hematopoietic bone marrow on ^{18}F-FDG PET and (d) on coronal ^{18}F-FDG PET/FSPGR (ellipse), (e) hypermetabolic hematopoietic bone marrow on fused ^{18}F-FDG-PET/STIR exams.
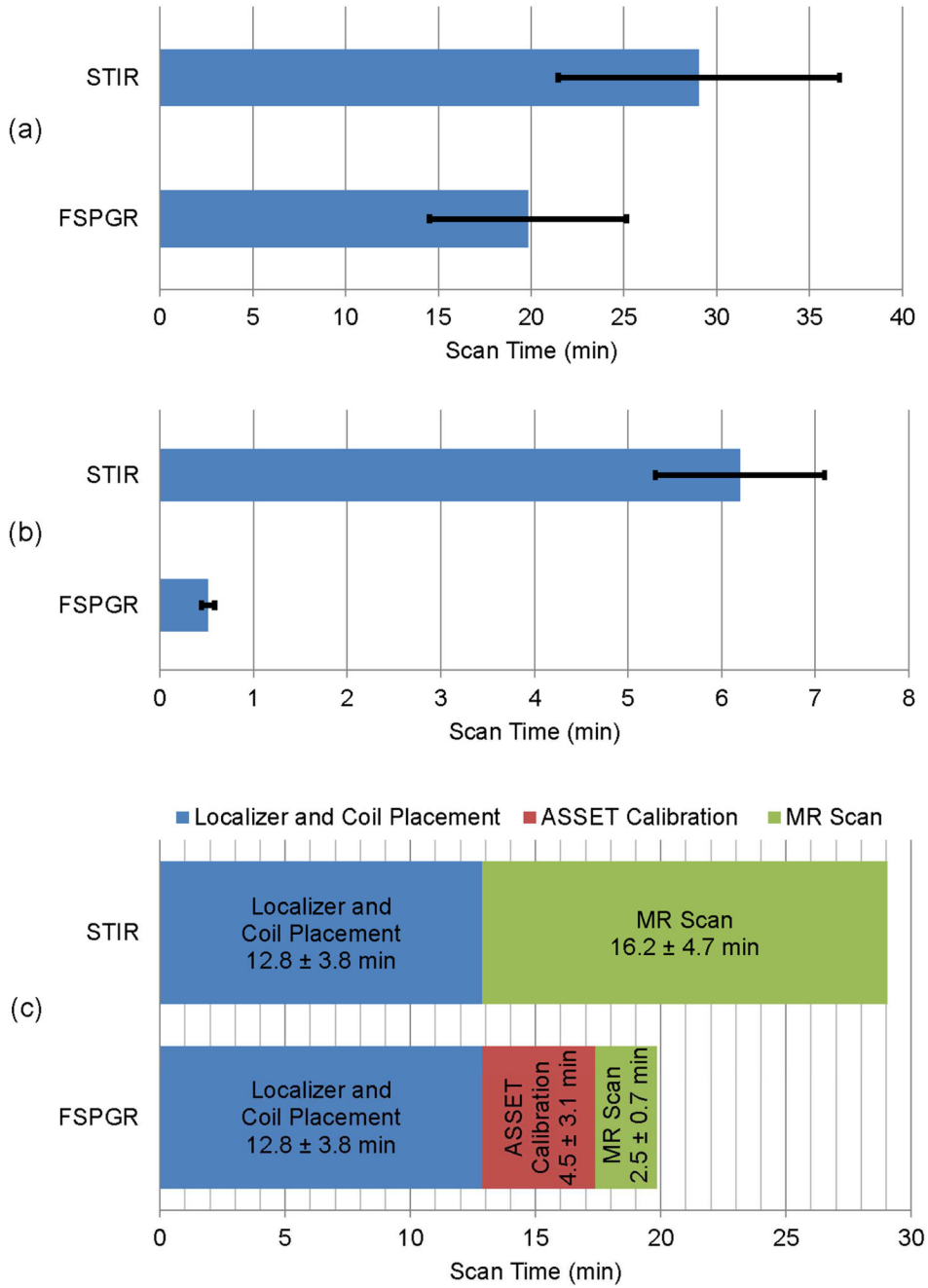
Fig. 4.
(a) Total scan-time of whole-body for FSPGR and STIR sequences, p = 0.001 indicates statistically significant difference based on a student's t-test. (b) MR scan-time per single anatomical site (such as chest, abdomen, pelvis or extremities) for FSPGR and STIR sequences, p < 0.001 indicates statistically significant difference based on a student's t-test, (c) Acquisition time for coil placement, localizer sequence, ASSET calibration and whole-body MR sequence. Data are displayed as means of 33 imaging studies and standard deviation.

Table 1

Patient information: patient age, gender and tumour type

No.	Gender	Age	Diagnosis
1	Male	10	Hodgkin's Lymphoma, stage IIIA
2	Female	10	Hodgkin's Lymphoma, mixed cellularity, stage III BS
3	Male	10	Osteosarcoma
4	Male	11	Hodgkin's Lymphoma, stage IIB
5	Female	11	diffuse large B-Cell lymphoma
6	Female	13	Hodgkin Lymphoma, nodular sclerosis subtype, stage IVA
7	Male	13	Burkitt Leukemia
8	Male	13	Hodgkin's Lymphoma, stage IV BE
9	Male	13	Hodgkin's Lymphoma, mixed cellularity, stage III BS
10	Male	13	Anaplastic Large Cell Lymphoma, stage III
11	Male	14	NK/T-cell lymphoma
12	Female	15	Hodgkin's Lymphoma, stage IIIAS
13	Male	15	Hepatosplenic gamma-delta T-cell Lymphoma with associated hemophagocytosis
14	Male	15	Hodgkin Lymphoma with bullky mediastinal disease, stage IVBS
15	Male	16	Hodgkin's Lymphoma, stage IIIB
16	Male	16	Hodgkin's Lymphoma, stage IIB
17	Male	16	Hodgkin's Lymphoma, stage IIIA
18	Female	16	Hodgkin's lymphoma
19	Male	18	nodular lymphocyte predominant Hodgkin's lymphoma, stage IIIA
20	Male	18	Osteosarcoma
21	Female	19	classical Hodgkin's lymphoma, stage IIIA
22	Female	19	Ewing Sarcoma
23	Male	20	Hodgkin's lymphoma
24	Male	20	Osteosarcoma
25	Male	20	Hodgkin's lymphoma
26	Male	21	B lympoblastic leukemia
27	Female	23	Ewing Sarcoma
28	Male	24	Hodgkin's Lymphoma
29	Male	25	Hodgkin's lymphoma
30	Male	26	Ewings Sarcoma
31	Male	26	Hodgkin's lymphoma
32	Male	29	grade 1–2 follicular lymphoma, FLIPI 2/5, stage IVAXS
33	Female	30	Hodgkin's Lymphoma, stage IA

Table 2

Comparison of ^{18}F-FDG PET/STIR and for ^{18}F-FDG PET/FSPGR for the detection of malignant lesions in children and young adults: Analysis based on 285 lesions at 2046 anatomical sites of 62 regions (nodal, extra-nodal and bone) assessed in 33 patients.

Regions		# of regions	Procedure	# of lesions	True Positive	False Positive	True Negative	False Negative	Sensitivity (%)	Specificity (%)	PPV (%)	NPV (%)	Accuracy (%)
	Head/Neck	5	PET/FSPGR	50	50	0	50	0	100	100	100	100	100
			PET/STIR	50	50	0	50	0	100	100	100	100	100
	Chest	11	PET/FSPGR	82	82	0	249	0	100	100	100	100	100
			PET/STIR	82	82	0	249	0	100	100	100	100	100
Nodal	Axilla	2	PET/FSPGR	18	18	0	35	0	100	100	100	100	100
			PET/STIR	18	18	0	35	0	100	100	100	100	100
	Abdominal	7	PET/FSPGR	30	30	0	177	0	100	100	100	100	100
			PET/STIR	30	30	0	177	0	100	100	100	100	100
	Pelvic	8	PET/FSPGR	25	24	1	200	0	100	99.5	96.0	100	99.6
			PET/STIR	25	24	1	200	0	100	99.5	96.0	100	99.6
Extra-nodal		10	PET/FSPGR	23	22	1	266	1	95.7	99.6	95.7	99.6	99.3
			PET/STIR	23	22	1	266	1	95.7	99.6	95.7	99.6	99.3
Bone		19	PET/FSPGR	58	57	1	402	1	98.3	99.8	98.3	99.8	99.6
			PET/STIR	57	57	0	403	1	98.3	100	100	99.8	99.8
Sum of all regions		62	PET/FSPGR	286	283	3	1380	2	99.3	99.8	99.0	99.9	99.7
			PET/STIR	285	283	2	1381	2	99.3	99.9	99.3	99.9	99.8

PPV: Positive Predictive Value, **NPV**: Negative Predictive Value